Renewable and Sustainable Energy Reviews 16 (2012) 3326–3338

Contents lists available at SciVerse ScienceDirect

Renewable and Sustainable Energy Reviews

journal homepage: www.elsevier.com/locate/rser

National geodatabase of tidal stream power resource in USA

Zafer Defne[a,*], Kevin A. Haas[a], Hermann M. Fritz[a], Lide Jiang[b], Steven P. French[c], Xuan Shi[c], Brennan T. Smith[d], Vincent S. Neary[d], Kevin M. Stewart[d]

[a] School of Civil and Environmental Engineering, Georgia Institute of Technology, 210 Technology Circle, Savannah, GA 31407, USA
[b] Center for Satellite Applications and Research, National Oceanic and Atmospheric Administration, Camp Springs, MD 20746, USA
[c] Geographic Information Systems, Georgia Institute of Technology, 280 Ferst Dr NW, Atlanta, GA 30332, USA
[d] Environmental Sciences Division, Oak Ridge National Laboratory, Oak Ridge, TN 37831, USA

ARTICLE INFO

Article history:
Received 5 August 2011
Accepted 20 February 2012
Available online 24 March 2012

Keywords:
Tidal energy
Tidal currents
Resource mapping
Numerical modeling
GIS

ABSTRACT

A geodatabase of tidal constituents is developed to present the regional assessment of tidal stream power resource in the USA. Tidal currents are numerically modeled with the Regional Ocean Modeling System (ROMS) and calibrated with the available measurements of tidal current speeds and water level surfaces. The performance of the numerical model in predicting the tidal currents and water levels is assessed by an independent validation. The geodatabase is published on a public domain via a spatial database engine with interactive tools to select, query and download the data. Regions with the maximum average kinetic power density exceeding 500 W/m^2 (corresponding to a current speed of ~1 m/s), total surface area larger than 0.5 km^2 and depth greater than 5 m are defined as hotspots and documented. The regional assessment indicates that the state of Alaska (AK) has the largest number of locations with considerably high kinetic power density, followed by, Maine (ME), Washington (WA), Oregon (OR), California (CA), New Hampshire (NH), Massachusetts (MA), New York (NY), New Jersey (NJ), North and South Carolina (NC, SC), Georgia (GA), and Florida (FL).

Contents

* Corresponding author. Tel.: +1 912 508 4572254.
E-mail addresses: zafer.defne@gatech.edu (Z. Defne), khaas@gatech.edu (K.A. Haas), fritz@gatech.edu (H.M. Fritz), lide.jiang@noaa.gov (L. Jiang), steve.french@coa.gatech.edu (S.P. French), xuan.shi@coa.gatech.edu (X. Shi), smithbt@ornl.gov (B.T. Smith), nearyvs@ornl.gov (V.S. Neary), stewartkm@ornl.gov (K.M. Stewart).

1364-0321/$ – see front matter © 2012 Elsevier Ltd. All rights reserved.
doi:10.1016/j.rser.2012.02.061

1. Introduction

In the past two centuries, the energy consumption per capita increased by a factor of 20, in excess of the six-fold increase in the world population. Presently, more than 80% of the global primary energy is met by fossil fuels, and only 13.5% by renewable resources [1]. A recent study estimates the global coal reserves to last for another century, while the oil and gas to be depleted within a few decades [2]. In addition, the increasing energy demand and the depletion rate of nonrenewable energy resources raise environmental concerns. For example, as a result of exploiting fossil fuels to meet the demand, CO_2 emission from electric power generation in the USA increased by 32% from 1990 to 2007 [3]. However, more than half the USA population lives within 80 km of coastlines, near tidal stream resources. Tidal streams, driven mainly by the gravitational force of the moon and sun, are highly predictable sources of renewable energy that may meet some of the energy demand without adding CO_2 emissions. The extent of their potential can be determined through an assessment of the scale of the available power and its spatial distribution. For this purpose, the tidal streams along the USA coasts are numerically modeled and an interactive geodatabase has been created to support further exploration.

According to the Assessment of Tidal Energy Resource guide by the European Marine Energy Centre Ltd (EMEC), tidal stream resource assessments may be categorized into four stages based on the extent and the detail of the assessment [4]. The first stage is the "Regional Assessment", which is an assessment on a regional or country level and aims at understanding the scale and characteristics of the tidal resource by performing numerical simulations. The second stage is the "Pre-Feasibility Study" which explores in detail the specific resource locations that are previously identified on a regional scale. Exploratory field surveys may accompany numerical simulations at this stage. For both of these stages, it is recommended to have a minimum simulation duration of 30 days with a minimum of 2 or 4 harmonic constituents forcing the models. A minimum grid resolution that is on the order of a few kilometers at the location of interest is satisfactory for a regional assessment, whereas grid points spaced less than 500 m are suggested for a pre-feasibility study. The third and fourth stages are the "Full-Feasibility Study" and the "Design Development" stages which include detailed economic models and development of the final design. These stages require a minimum of 8 constituents to drive the model, longer periods of simulations and longer records from field surveys, and an order of magnitude finer grid spacing. The impacts of the power extraction also need to be addressed at these stages. The scope of this study is to provide a regional assessment, yet the modeling is done at a pre-feasibility study level. Instead of field campaigns, data reported in the literature are used for model calibration and validation.

The "available power" is defined as the power that is associated with the undisturbed, natural flow conditions. It is different than the "absorbed power" (aka dissipated power), which is the power removed from the system by a converter or the "captured power" (aka extracted power), which is the useful power delivered by it. The final modeling results are stored in a geodatabase, a data repository specifically designed to store and query geospatial data. The U.S. Department of Energy keeps an inventory of reports and digital maps of national renewable resource that provide information on the scale and spatial distribution of various resources such as wind, solar, geothermal, hydropower and biomass [5]. Despite being static images, these maps constitute a good source of regional assessment when combined with the reports. However, the previous lack of a full spatial–temporal assessment of tidal currents for the USA is a barrier to the comprehensive development of tidal current energy technology. The recent efforts include a series of reports by the Electric Power Research Institute, EPRI [6], which are limited to few representative sites; and a few other isolated cases for planned local projects [7]. By creating a national database of tidal stream energy potential, as well as an interactive GIS tool usable by the industry in order to accelerate the market for tidal energy conversion technology, the present study is an addition and improvement to the inventory of renewable resources.

The development stages described here include numerical modeling of tidal streams, calibration of the model for each grid, validation of the model results, development of the geodatabase and dissemination of data to the public.

2. Numerical modeling of tidal streams

The tidal stream modeling is based on Regional Ocean Modeling System (ROMS). The coast is divided into a number of individual subdomains for modeling, and the results for water levels and depth integrated tidal currents are used to calibrate the model against the available data for each subdomain.

2.1. Model set-up

ROMS is a member of a general class of three-dimensional, free surface, terrain following numerical models that solve three dimensional Reynolds-averaged Navier–Stokes equations (RANS) using the hydrostatic and Boussinesq assumptions [8]. ROMS uses finite-difference approximations on a horizontal curvilinear Arakawa C grid and vertical stretched terrain-following coordinates. Momentum and scalar advection and diffusive processes are solved using transport equations and an equation of state computes the density field that accounts for temperature, salinity, and suspended-sediment concentrations. The modeling system provides a flexible framework that allows combinations of various components depending on user needs. In this study, the model is run in multiple processors using distributed-memory, with a three-dimensional barotropic configuration for simulating the tides. The computational grids are set up and the results are calibrated following the outlines of tidal stream modeling efforts for a regional study [9].

The USA coastline is divided into 52 subdomains with an average grid spacing of 350 m as shown in Fig. 1. The only exception is the Puget Sound grid for which the results from an earlier study are used [10]. The coastline data, used for masking the land nodes, is obtained from the National Ocean Service (NOS) Medium Resolution Coastline via the Coastline Extractor [11] and processed in MATLAB to fill in gaps. Raw bathymetry is obtained from the NOS Hydrographic Surveys Database [12]. The bathymetry data in the NOS database are generally referenced to Mean Lower Low Water (MLLW) while ROMS bathymetry is defined with respect to Mean Water Level (MWL) or Mean Tidal Level (MTL). A conversion from MLLW to MTL referenced values is performed based on the data provided by the National Oceanic and Atmospheric Administration (NOAA) at the tidal stations [13] or NOAA Vertical Datum Transformation software (VDatum) [14]. Supplementary data to replace missing bathymetry points are acquired from NOAA Electronic Navigational Charts [15] and National Geophysical Data Center Geophysical Data System database (GEODAS) [16].

The additional water volume supplied by the wetlands is implemented in the computational model through the wet-dry module in ROMS, which allows for computational nodes to be defined as land or sea nodes dynamically with respect to the water content. Wetland boundaries are acquired from the National Wetland Inventory of the US Fish & Wildlife Services [17]. Elevation data for wetlands is cropped from the one-arc second topography data downloaded from USGS Seamless Server [18]. The topography data is referred

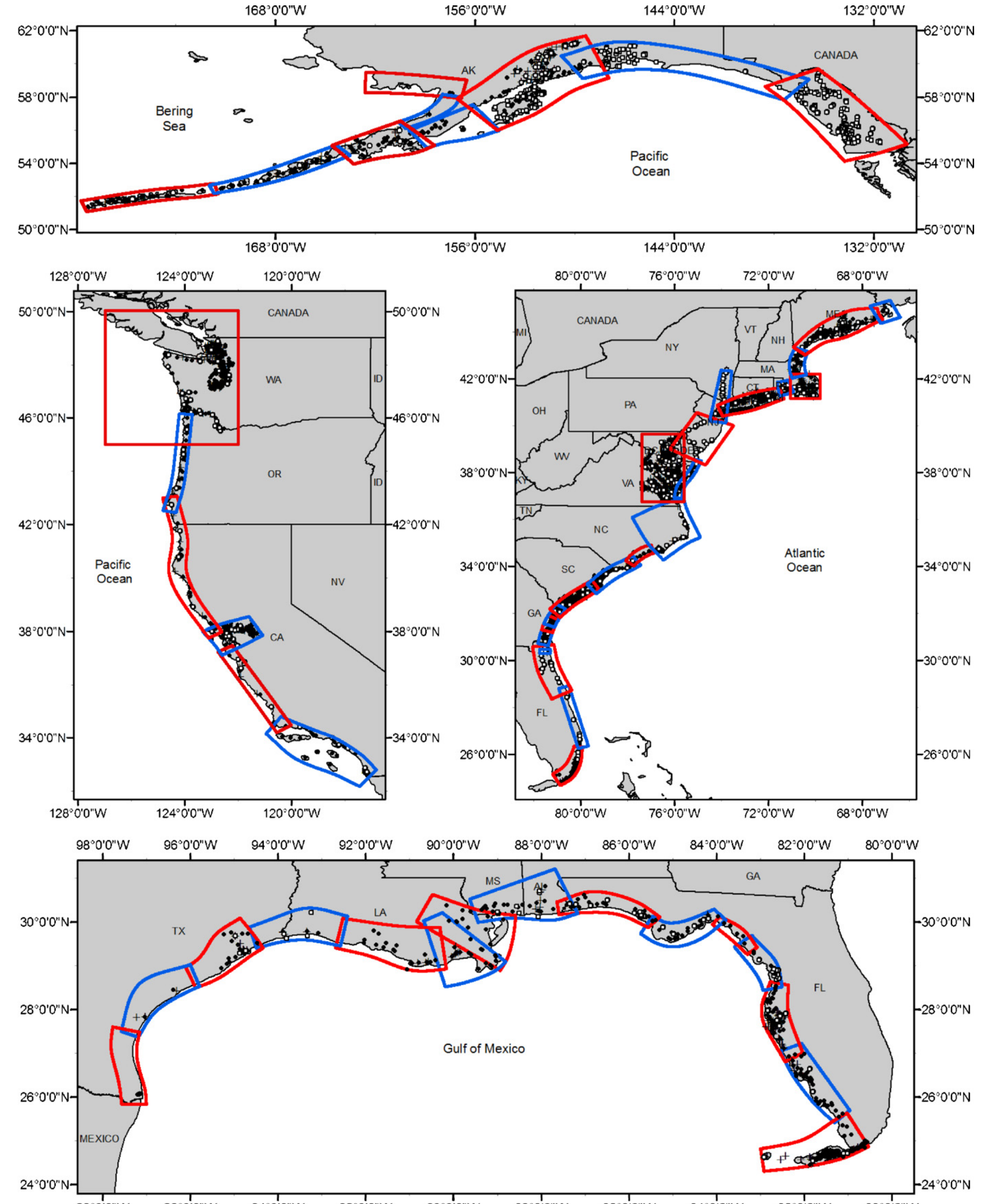


Fig. 1. Map of computational grids and the calibration data sources. Harmonic constituents for tidal currents (□) and water levels (○), and prediction for maximum current (+) and high/low tide elevations (●).

to NAVD88. The data is converted to MTL reference via interpolating from NOAA tidal stations datum in the model domain or VDatum where available. After conversion, the sea bathymetry and the wetland topography are merged into a single set of points before constructing the computational grids. The Seagrid MATLAB package is used to generate the model grids [19]. A spatially uniform quadratic bottom friction used for each grid.

Tidal constituents are periodic oscillations driven by the celestial forces computed with the mathematical approximation of the astronomical tides given as

$$H = a_0 + \sum_{i=1}^{N} a_i \cos(\sigma_i t + \delta_i) \quad (1)$$

where H is the astronomical tide at time t since the start of the tidal epoch, a_0 is the vertical offset, a_i, σ_i, δ_i are the amplitude, angular frequency and phase angle of the ith tidal constituent [20]. For the USA East coast and the Gulf of Mexico, the ROMS tidal forcing file is generated by interpolating the ADCIRC [21] tidal database at the open boundary nodes of the ROMS grid. The harmonic constituents used for the forcing includes Q1, O1, K1, S2, M2, N2, K2, M4 and M6. For the USA West coast and Alaska domains, TPXO data [22], with the constituents Q1, O1, K1, S2, M2, N2 and M4 are used. Stream flow data for is obtained from the USGS National Water Information System [23] for the Mississippi River and yearly average discharges are applied as a point source at the river boundary. Open boundary conditions are defined in all of the grids as free-surface Chapman condition [24] for the tidal elevation, Flather condition [25] for barotropic velocity (2D momentum), and gradient (aka Neumann) condition for baroclinic velocity (3D momentum) [26]. The results from 30-day simulations are used in the analyses after running the model for 32-day simulations with 2 days for the spin-up.

2.2. Model calibration

The calibration procedure begins with a full 32 day model run which is then compared with the data. Based on a holistic approach about the general trend of over versus under predictions for all the various stations in the domain, the model parameters such as the friction factor are modified uniformly for the entire grid and a shorter model run consisting of 7 days is completed. The relative changes in the currents are evaluated, and this process is repeated until the desired accuracy is obtained. Finally, another 32 day model run is completed with the selected parameter values for the creation of the final harmonic constituents. The calibration data includes the in situ measurements collected from various sources, harmonic constituents and as well as the high/low tide or maximum/minimum current predictions from NOAA Tides & Currents. If measurements with a duration longer than a month are available, harmonic constituents are extracted from both model and data to be compared. Both magnitude and phase are calibrated by adjusting the friction factor for the regional model until reasonable agreement between predicted and measured harmonic constituents is achieved. If the calibration data contain only high/low tides or maximum/minimum currents, the extreme values are extracted from the model for calibration. Harmonic constituent calibrations are preferred over extreme value calibrations, since the harmonic constituents are obtained from measurement sites and may be more reliable than the predicted extreme values. Therefore, extreme value calibrations are only used when there are few or no measurements sites in the region.

The calibration parameters regarding the harmonic constituents of tidal elevations, harmonic constituents of tidal currents and predicted maximum/minimum tidal currents and predicted high/low tides are explained below.

2.2.1. Harmonic constituents for tidal currents

2.2.1.1. Amplitude difference (amd). This parameter is an estimation of how much the model underpredicts ($amd < 0$) or overpredicts ($amd > 0$) the amplitude of the kth harmonic constituent. It is given by

$$amd_k = (amp_m)_k - (amp_c)_k \quad (2)$$

where $(amp_m)_k$ and $(amp_c)_k$ are the combined amplitudes of the kth harmonic constituent computed by the model output and the calibration data, respectively. The combined amplitude for each harmonic constituent is calculated as the square root of the squares of major and minor axes of the tidal ellipse, given by

$$amp = \sqrt{a_{maj}^2 + a_{\min}^2} \quad (3)$$

where a_{maj} and a_{min} are the major and the minor axis amplitudes of the tidal ellipse. The combined amplitude is not an observed parameter but a synthetic one that facilitates a combined assessment of major and minor axis amplitude differences.

2.2.1.2. Percentage amplitude difference (amdp). A dimensionless parameter that gives the percent underprediction ($amdp < 0$) or overprediction ($amdp > 0$) of the amplitude of the kth harmonic constituent as given in Eq. (4).

$$amdp_k = \frac{(amp_m)_k - (amp_c)_k}{(amp_c)_k} \times 100 \quad (4)$$

2.2.1.3. Tidal ellipse inclination difference (incd). The difference between the inclination of the tidal ellipses calculated by the model and the measurements is given by

$$incd_k = (inc_m)_k - (inc_c)_k \quad (5)$$

where $(inc_m)_k$ and $(inc_c)_k$ are the orientation of the tidal ellipse (measured in degrees, anti-clockwise from East to the semi-major axis of a tidal ellipse) of the kth harmonic constituent computed by the model output and given in data, respectively.

2.2.1.4. Phase difference (phd). Phase difference indicates how much the model output lags ($phd > 0$) or leads ($phd < 0$) the given data for each of the modeled harmonic constituent for water surface level and is given by

$$phd_k = (pha_m)_k - (pha_c)_k \quad (6)$$

where $(pha_m)_k$ and $(pha_c)_k$ are the phases of the kth harmonic constituent in minutes computed by the model output and given in data, respectively.

2.2.2. Harmonic constituents for water level

The calibration parameters for the harmonic constituents for water levels include amplitude difference (amd), percentage amplitude difference ($amdp$) and phase difference (phd) and are defined in the same manner with the calibration parameters for the harmonic constituents for tidal currents.

Statistics of the calibrated final results from two points at Cook Inlet in Alaska are given here as an example. The comparison of the tidal current constituents derived from measurement data and model results on the east of Kalgin Island is shown in Table 1. According to the measurements the combined amplitude (amp_c) for major constituent M2 at this location is 1.66 m/s. The model estimate, amp_m, is 0.18 m/s smaller than this value, which corresponds to an 11% difference ($amdp = -11\%$). The percentage amplitude difference is larger for S2 and K1 than M2 although they translate to a much smaller amplitude difference between the measurements and the model results. The tidal ellipse inclination from the

Table 1
Comparison of the tidal current constituents derived from measurement data and model results on the east of Kalgin Island at Cook Inlet, AK (151.6732°W, 60.4830°N).

Constituent	Period (h)	*amp* (m/s)	*amd* (m/s)	*amdp* (%)	*inc* (°)	*incd* (°)	*phd* (min)
M2	12.4206	1.66	−0.18	−11	73	3	−43
S2	12	0.38	0.10	27	73	−2	12
K1	23.9345	0.32	−0.08	−26	73	1	54
N2	12.6583	0.31	−0.02	−6	73	−4	−39
O1	25.8193	0.13	0.01	8	73	−10	45
M4	6.2103	0.12	−0.07	−56	65	11	−120
M6	4.1402	0.09	−0.08	−82	73	−20	94
Q1	26.8684	0.01	0.01	164	83	−40	530

Table 2
Comparison of the water level constituents derived from measurement data and model results near Nikiski at Cook Inlet, AK (151.4053°W, 60.6810°N).

Constituent	Period (h)	*ampc* (m)	*amd* (m)	*amdp* (%)	*phd* (min)
M2	12.4206	2.5	−0.17	−7	−25
S2	12	0.86	−0.04	−5	−4
K1	23.9345	0.64	−0.05	−8	11
N2	12.6583	0.5	−0.01	−2	−6
O1	25.8193	0.38	0.01	2	25
M4	6.2103	0.09	0.03	35	−9
M6	4.1402	0.07	0	−2	−12
Q1	26.8684	0.06	0	4	−8

model for M2 is 3° larger than the measured value at this location. The phase differences are found to be under an hour for the first five major constituents, which is acceptable since the model output is recorded hourly. It is noted that as the amplitude of the constituent starts to diminish the error in phase can increase significantly (e.g. 530 min for Q1). However, this does not impose a major problem when the amplitude is negligibly small. The calibration process involves overall evaluation of results from every measurement point in a given computational grid. The results for combined magnitude of M2 tidal current constituent for Cook Inlet are shown in Fig. 2, which shows that the model can be overpredicting or underpredicting when the results are within an acceptable range. The average absolute difference between the model and the measurements in Cook Inlet for the combined amplitude and the tidal ellipse inclination are 19% and 13%, respectively.

The final calibration statistics for the water level constituent near Nikiski, AK (Table 2) shows that the model prediction for the amplitude of the major constituent M2 is 0.17 m less than the measured amplitude of 2.5 m (*amd* = −0.17 m). The percentage amplitude difference, *amdp*, is −7% for M2 and its absolute value remains below 10% for all other constituents with the exception of M4. However, the larger percent difference in the M4 amplitude corresponds to a few centimeters since the amplitude of M4 is considerably small. The modeled and measured magnitudes of the M2 tidal constituent for Cook Inlet are shown in Fig. 3. The model slightly overpredicts the measured M2 amplitudes for this grid, with an average of 10%. This is considered acceptable within the scope of a regional assessment. The phase differences are less than 30 min and slightly better than the results for tidal currents. Overall, the water level calibration statistics are better than tidal current calibration statistics, which is a general trend observed throughout the entire data set.

2.2.3. Predicted maximum currents

2.2.3.1. Mean current magnitude ratio of maximum currents (cmgrt). The average ratio of the predicted maximum current magnitudes

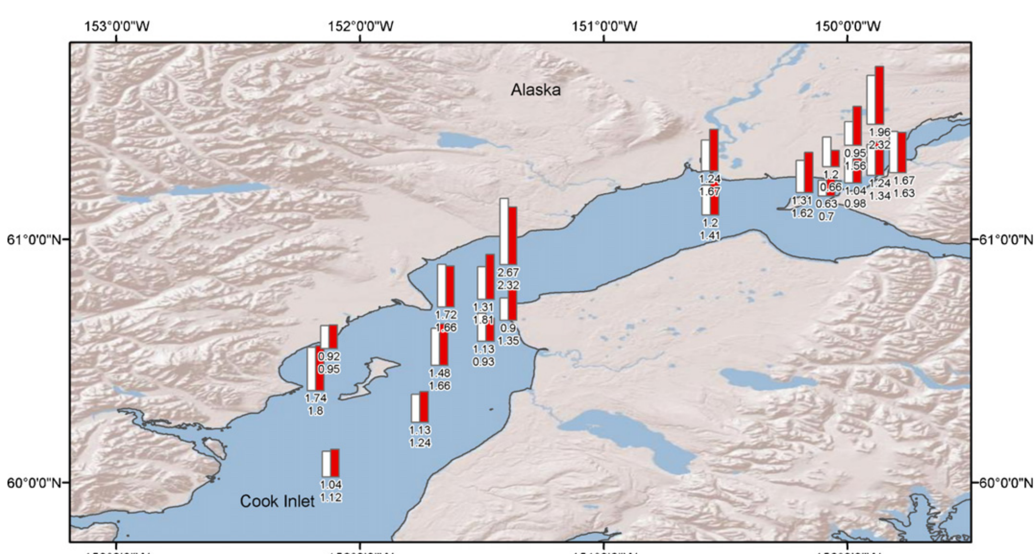


Fig. 2. Comparison of combined amplitude (m/s) of M2 tidal current constituent calculated from the model (white) and measurements (red) for the Cook Inlet, AK. The model (top) and the measurement (bottom) values are marked at every site. (For interpretation of the references to color in this figure legend, the reader is referred to the web version of the article.)

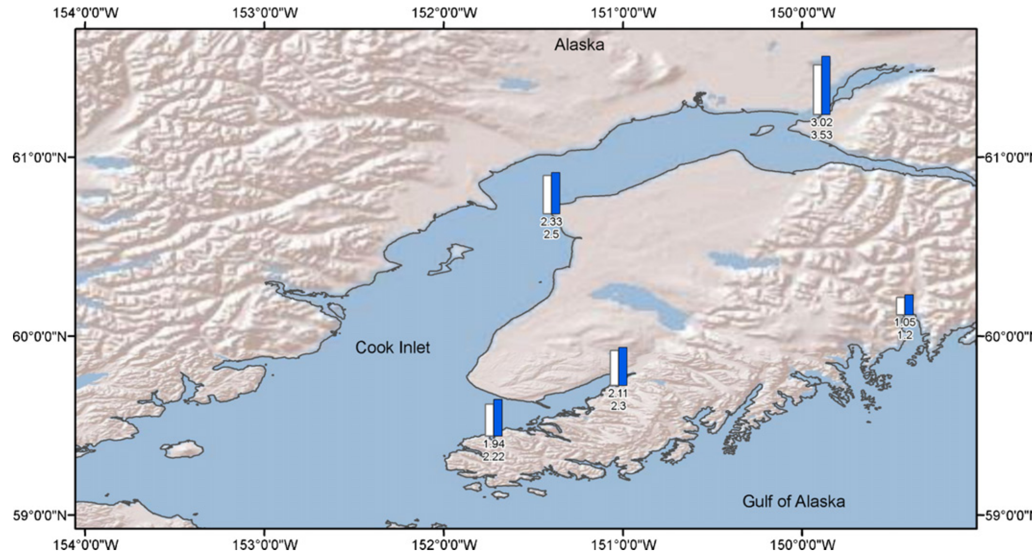


Fig. 3. Comparison of amplitude of water level constituent (m) for M2 tidal constituent calculated from the model (white) and measurements (blue) for the Cook Inlet, AK. The model (top) and the measurement (bottom) values are marked at every site. (For interpretation of the references to color in this figure legend, the reader is referred to the web version of the article.)

from the model to the magnitudes of the corresponding predicted maximum current values from the calibration data is given by

$$cmgrt = \frac{\sum_{i=1}^{N}(|(cur_m)_i|/|(cur_c)|_i)}{N} \quad (7)$$

where cur_m is the maximum current magnitude from the model and cur_c is the predicted maximum current value, and i and N are the ith occurrence and total number of occurrences of maximum and minimum during the simulation duration, respectively.

2.2.3.2. Root-mean-square difference of maximum currents (crms). This parameter, given with Eq. (8), is the root-mean-square of the difference between the maximum current values output by the model and maximum current values from the data and is an estimate for the error in predicting maximum current magnitude.

$$crms = \sqrt{\frac{\sum_{i}^{N}\{(cur_m)_i - (cur_c)_i\}^2}{N}} \quad (8)$$

2.2.3.3. Phase difference between maximum currents (cpd). The mean phase difference for maximum currents and the mean phase difference for maximum flood and ebb currents is given by

$$cpd = \frac{\sum_{i=1}^{N}\{(t_m)_i - (t_c)_i\}}{N} \quad (9)$$

where t_m and t_c are the times that correspond to the maximum tidal current occurrences in the model output and the calibration data, respectively. Current phase difference is an estimate to how much phase the model output lags ($cpd > 0$) or precedes ($cpd < 0$) the calibration data.

2.2.4. Predicted high/low tides

2.2.4.1. Standard deviation ratio of high/low tides (stdrt). An estimate of how much the model underpredicts ($stdrt < 1$) or overpredicts ($stdrt > 1$) the tidal range, the ratio between standard deviation of the high/low tide computed with the model and predicted by NOAA is given by

$$stdrt = \frac{\sqrt{\left(\sum_{i=1}^{N}\{(elv_m)_i - \overline{elv_m}\}^2\right)/N}}{\sqrt{\left(\sum_{i=1}^{N}\{(elv_v)_i - \overline{elv_c}\}^2\right)/N}} \quad (10)$$

where elv_m and elv_c are the high/low tide time series from the model and the data.

2.2.4.2. Root-mean-square difference of high/low tides (rms). The root mean square difference between the model output and NOAA predictions for high/low tides as given in Eq. (11).

$$rms = \sqrt{\frac{\sum_{i=1}^{N}\{(elv_m)_i - (elv_c)_i\}^2}{N}} \quad (11)$$

2.2.4.3. Phase difference between high/low tide (phd). These terms estimate how much the model output lags ($phd > 0$) or leads ($phd < 0$) the change in the water surface level during tides. It is calculated with the same equations for currents by using the high and low tide times.

Calibration statistics of model results with NOAA predictions for maximum currents are demonstrated with examples from St Catherines Sound in Georgia in Table 3. This location has moderate tidal currents with an average magnitude for maximum current predictions by NOAA being less than 1 m/s. It is seen that the model usually overpredicts the magnitude of maximum tidal current at this particular location. However, the data shown here covers only a small part of the computational grid that includes several sounds for which the results also include underpredictions. For this specific example, depending on the location the mean current magnitude ratio (*cmgrt*) can be as high as 1.32 with a *crms* of 0.39 m/s, although higher values may be found within the complete set of data. The large differences for the maximum current predictions can be attributed to many reasons. In addition to correct prediction of the currents being more challenging than water levels, comparing the results with predictions rather than directly to measurements introduces some ambiguity. Having only the maximum predicted values to compare against can contribute to larger differences. On the other hand, although the magnitude differences can

Table 3
Maximum current predictions at St. Catherines Sound and Newport River, GA.

Station name	Longitude (°)	Latitude (deg)	Mean of maximum current (m/s)	*cmgrt* (–)	*crms* (m/s)	*cpd* (min)
St. Catherines Sound Entrance	−81.1405	31.7150	0.94	1.32	0.39	33
Medway River, northwest of Cedar Point	−81.1908	31.7145	0.82	1.36	0.44	−52
N. Newport River, NE of Vandyke Creek	−81.1870	31.6912	0.82	1.29	0.42	52
N. Newport River, above Walburg Creek	−81.1953	31.6738	0.75	1.00	0.25	−49
N. Newport River, NW of Johnson Creek	−81.2105	31.6630	0.74	1.17	0.32	−23
N. Newport River, ESE of S. Newport Cut	−81.2645	31.6653	0.64	1.41	0.35	10

vary largely, the phase differences for the maximum current speed are generally on the order of an hour for the entire data set. For the locations considered in this case it is calculated to be slightly larger than half an hour.

The tidal range in St. Catherine Sound, GA is predicted to be slightly larger than 2 m for the locations displayed in Table 4, based on the high/low water predictions by NOAA. According to the calibration statistics for high/low water level, the average root-mean-square difference in high/low tides (*rms*) at these locations is approximately 0.14 m, which is satisfactory for the given tidal range. The standard deviation ratio of high/low tides (*stdrt*) is slightly less than 1.0 at all of the locations, indicating that the modeled tidal range is slightly smaller than the NOAA predictions. The modeled high/low tides are found to lead the predictions nearly by half an hour.

The NOAA predictions are calculated from constituents obtained from short measurements at relatively small numbers of tidal stations. These predictions are then translated to larger numbers of subordinate stations through specific calculations by NOAA. Consequently, the predictions are less reliable than the actual measurements, hence they are only used for calibration when there is no measured data available. Nevertheless, when both sources are available, the final calibration statistics for both are published together with the measurement data even if they are not used in calibration. The only exception to this is the Cook Inlet, where the comparisons with the predictions are omitted since the measurement data are abundant.

3. Assessment of tidal stream resource

Final results are obtained after each model grid is run consecutively. The independent validation by ORNL and the calculation of stream power density are described below.

3.1. Validation of model results

The model performance in predicting tidal elevation and depth-averaged velocity are independently validated by the Oak Ridge National Laboratory (ORNL) at locations where true values are assumed to be point measurements from tidal monitoring stations [27]. The validation methodology focuses on comparing the time-series of the current speeds and elevations as opposed to comparing tidal constituents. The model time series are constructed from the final constituent database and compared to the measured time series. Two classes of point measurements are defined for the validation purpose: Class 1 validation is a split sample validation commonly used to evaluate the performance of a calibrated model with measurements independent of those used for calibration, whereas Class 2 validation is an assessment of the model calibration procedure using different performance metrics [27] than those described here. More than fifty measurement stations are selected for validation based on (1) Various levels of power densities; (2) vicinity to larger population and cities; and (3) representative of several different areas along the USA coast. Correlation statistics, including phase shift, amplitude ratio, and coefficient of determination (R^2) values are calculated along with model performance metrics that include the root mean square error, Nash–Sutcliffe efficiency coefficient, and mean absolute error. Model predicted and measured depth-averaged current speed frequency and cumulative frequency histograms, means, standard deviation and maximum and minimum values are compared. Further information about the validation procedure and detailed results are available in the original validation report by ORNL [27].

Following the EMEC guidelines for a regional assessment, model predictions are considered adequate when predicted maximum current speeds are within 30% of those estimated from tidal monitoring station measurements. The validation results indicate that the model predicts current speeds and tidal elevations with R^2 values ranging from 0.76 to 0.80 and from 0.79 to 0.85, respectively. The model has a slight tendency to over predict mean and maximum current speeds for medium to high power density regions and a tendency to under predict speeds in low power density regions. Based on the comparison of measured and model predicted current speeds, for both classes of stations located in the medium to high power density regions, the model over predicts mean and maximum current speeds by 24% and 21% on average, respectively. Similarly, for those stations that are under predicted, they are done so by −18% on average for the mean current speeds and −13% on average for the max current speed. The model performance for the prediction of tidal elevations is found to be better than the tidal currents.

Since the actual time series from measurements are used in validation, any effects related to wind driven flow and fresh water intrusion and even localized effects caused by local flooding in tidal rivers can compromise the validation results. In addition, the validation procedure recognizes the limitations of regional assessment models with coarse grid resolution to predict local variations in current speed and tidal elevation within 300–500 m parcels. Model performance evaluations are therefore restricted since model predicted values that are spatially averaged over a 300–500 m grid cell cannot be expected to correspond with tidal monitoring station measurements taken at a point at a given latitude and longitude. Tidal currents at places like Admiralty Inlet in WA have been shown to vary greatly over scales less than 500 m [28]. Overall, the model

Table 4
High/low water elevation predictions at St. Catherines Sound and Newport River, GA.

Station name	Longitude (°)	Latitude (°)	Mean of high water (m)	Mean of low water (m)	*stdrt* (–)	*rms* (m)	*phd* (min)
Walburg Creek entrance	−81.3667	31.5500	1.10	−0.97	0.93	0.15	−28
Bear River Entrance	−81.3167	31.4833	1.10	−0.95	0.92	0.16	−27
North Newport River	−81.4667	31.3333	1.20	−1.01	0.95	0.13	−32
South Newport Cut, N. Newport River	−81.4000	31.3000	1.15	−1.02	0.97	0.11	−43

predictions are found to be satisfactory for regional assessments of tidal stream power potential.

3.2. Tidal stream power density hotspots

The tidal stream power is evaluated by computing the kinetic power density from the tidal current speeds using

$$P = \frac{1}{2}\rho V^3 \quad (12)$$

where P is the tidal stream power per unit area of flow, i.e. tidal stream power density, ρ is the density of seawater and V is the current speed. The recent tendency towards the use of open turbines rather than tidal barrages, and the characteristics of the existing tidal stream power conversion technology bounded by minimum current speed requirements for power take-off favor the identification of hotspots based on the kinetic power of the tides rather than their potential power. Stronger tidal streams mean faster currents, which corresponds to a cubical increase in power density. The overall power that can be converted from tidal streams is a function of both the kinetic and potential energy, with other additional parameters such as the site characteristics, device characteristics and environmental impacts which further complicate the calculation of the ultimate resource potential. For the sake of clarity, we consider solely the tidal stream power density as an indicator of hotspots. Calculation of the ultimate capacity of the resource at these hotspots requires further investigation of these sites on a case by case basis.

On the other hand, a regional assessment is well suited for the purpose of site screening. In addition, minimum current speed and minimum depth requirements can be imposed in order to narrow down the number of hotspots. Generally, tidal stream power converters require a minimum flow speed (cut-in speed) to start operating, which ranges from 0.5 m/s to 1 m/s depending on the design. Although some studies that simulate power extraction acknowledge cut-in speed values for the horizontal axis turbines as large as 1 m/s [29,30], there are many examples with cut-in speeds around 0.7 m/s and a vertical axis turbine with 0.5 m/s [31–33]. In this study, the minimum for the power density is selected as 500 W/m^2 which corresponds to a flow speed of ∼1 m/s. If the maximum of the mean kinetic power does not exceed 500 W/m^2 within the boundaries of the hotspot area the hotspot is excluded from the list. Regardless of their design, the tidal stream power converters also require a minimum depth that allows for allocating the device with enough top and bottom clearance. The dimensions of tidal stream power devices change from several meters to tens of meters [32,34]. Since the analysis in this study does not depend on a specific device the minimum depth is chosen to be 5 m, large enough to accommodate a small size conversion device with the existing technology. Finally, the list of hotspots is filtered with a minimum surface area requirement of 0.5 km^2. The surface area does not contribute to power density, but is required in order to accommodate larger space for development. This final filter also reduces the number hotspots list by removing more than two thirds of the initial list. Based on these criteria, the geospatial data along the USA coasts has been filtered to define the hotspots with notable tidal stream power densities, which are listed in Table 5. The coordinates of each hotspot location, maximum and average depth with respect MLLW, and surface area of these regions are given together with the largest mean power density within each location. For brevity, the listed locations mark the general vicinity of the hotspots and do not necessarily pinpoint the exact location of each hotspot individually. For further analysis the reader is suggested to visit the original geodatabase [35].

Alaska (AK) has the largest number of hotspots and some of the largest kinetic power densities in the USA according to the list. Cook Inlet represents one of the best resources of tidal stream power with a surface area that is an order of magnitude larger than the rest of the hotspots and a substantially large kinetic power density,. The largest kinetic power density locations within AK include Bristol Bay, Akutan, Unalga and Samalga Passes, Sikitnak Island, Turnagain Arm; and Kopreanof, Icy and Peril Straits. Maine (ME), Washington (WA), Oregon (OR), California (CA), New Hampshire (NH), Massachusetts (MA), New York (NY), New Jersey (NJ) North and South Carolina (NC, SC), Georgia (GA), and Florida (FL) have the next largest tidal stream power potential. Tacoma Narrows, Rosario Strait, Bellingham Channel in WA, Nantucket Sound and Western Passage in ME are some of the hotspots with large kinetic power density. The list provided in this study includes the top tier tidal stream power density hotspots at a national resource assessment scale based on numerical modeling of the tidal currents and after certain filtering. There are many locations that are excluded as a result of applied filters, however, they can be found in the original geodatabase. Some of the filtered locations with tidal power density still greater than 250 W/m^2 include, but not limited to Cape Cod Canal in MA; Hudson River in NY; Great Egg Harbor Bay in NJ; Cape Fear in NC; Charleston Harbor, Port Royal Sound, Cooper and Beaufort Rivers in SC; St Johns River in FL; Carquinez Strait, Eel and Siltcoos Rivers in CA, Mud Bay Entrance and Cooper River Delta in AK. There may also be additional locations that are viable for tidal stream power conversion, but which are not resolved by the numerical model. These are probably local resources that can only be detected through finer modeling at smaller scales or with field measurements such as the Kootznahoo Inlet in AK; Willapa Bay in WA; Sheepscot Bay in ME; Shelter Island Sound in NY; Manasquan River in NJ.

4. Dissemination of data

The final results at each grid point are stored in a database with 67 fields that display geographical coordinates, the modeled depth, computed water level constituents and tidal current constituents, and one-month mean/maximum for tidal current speed and tidal stream power density. The information regarding the constituents includes the constituent name, amplitude and phase (with respect to Greenwich) for water level; a major and a minor axis amplitude, phase and inclination angle for the tidal current. The final data is published on a public interactive map at http://www.tidalstreampower.gatech.edu/.

The entire suite of data is stored in a geodatabase and made public via the ArcGIS server. All of the edits are transferred and synchronized with the data on the production geodatabase, which is accessible by multiple editors and then copied to a publication geodatabase for dissemination. The web page interface is a rich Internet application (RIA) that facilitates easy navigation over the map with options for alternative views [35]. Users can interact with the map using the pull down menus or widgets on the right of the screen (Fig. 4). A highlight of the web page functions are presented here.

4.1. Data layers

The web page consists of multiple layers (a data points layer and a set of color mapped raster layers) that can be turned on and off with the data layers widget. The color mapped raster layers include the water depth, the mean current speed (one month average of depth integrated tidal current speed) and the mean kinetic power density (one month average of kinetic power density based on depth integrated tidal current speed). These layers are generated by interpolating the model results from computational grids onto an ArcGIS raster grid with 0.003° resolution and are useful

Table 5
Locations and characteristics of the tidal stream density hotspots along the coast of USA.

State	Hotspot	Location (°N, °W)	Surface area (km^2)	Maximum depth (m)	Mean depth (m)	Kinetic power density (W/m^2)
ME	Coobscook Bay	(44.891, 67.107)	<1	17	14	574
ME	Lubec Channel	(44.853, 66.977)	<1	8	7	891
ME	Grand Manan Channel	(44.8, 66.892)	21	101	79	768
ME	Western Passage	(44.911, 66.977)	7	106	43	7366
ME	Knubble bay	(43.882, 69.731)	<1	14	11	730
ME	Hockmock Bay	(43.902, 69.737), (43.912, 69.718)	<1, <1	12, 7	7, 6	1747, 567
ME	Kennebeck River	(43.93, 69.81), (43.969, 69.825)	<1, <1	7, 8	7, 8	552, 528
ME/NH	Piscataqua River	(43.073, 70.728), (43.092, 70.775), (43.113, 70.807)	2, 1, <1	20, 17, 13	13, 12, 9	2823, 2633, 1239
MA	Nantucket Sound	(41.197, 69.902), (41.345, 70.396)	398, 202	38, 39	16, 10	7328, 4844
MA	Vineyard Sound	(41.499, 70.647), (41.362, 70.854)	137, 2	33, 24	19, 15	3344, 603
NY	Block Island Sound	(41.229, 72.061), (41.167, 72.21), (41.075, 71.845)	7, 2, 4	85, 49, 15	38, 21, 12	740, 610, 530
NY	East River	(40.79, 73.935), (40.775, 73.937), (40.706, 73.979)	<1, <1, <1	5, 1, 11	5, 6, 11	547, 1546, 768
NJ	Delaware Bay	(38.921, 74.963)	11	13	9	913
NC	Cape Hatteras	(35.185, 75.762)	<1	9	8	1378
NC	Portsmouth Island	(35.068, 76.016)	3	10	7	911
SC	Cooper River	(32.88, 79.961)	<1	8	7	830
SC	North Edisto River	(32.576, 80.2)	7	19	12	1008
SC	Coosaw River	(32.492, 80.49)	12	17	10	566
GA	Ogeechee River	(31.856, 81.118)	1	8	7	834
GA	Altamaha River	(31.319, 81.309)	1	8	6	511
GA	Satilla River	(30.97, 81.505)	<1	8	7	606
GA/FL	St Marys River	(30.707, 81.445), (30.721, 81.508)	5, <1	20, 8	12, 6	798, 705
FL	Florida Keys	(24.692, 81.143), (24.681, 81.168), (24.574, 81.839), (24.556, 82.056)	3, 1, 10, 29	10, 7, 11, 10	6, 6, 7, 6	992,643, 904, 538
FL	Port Boca Grande	(26.716, 82.251)	<1	20	10	1140
FL	St Vincent island	(29.625, 85.101)	<1	11	8	625
CA	Golden Gate	(37.822, 122.471)	<1	111	50	750
CA	Carquinez Strait	(38.036, 122.158)	12	36	19	914
CA	Humbolt Bay Entrance	(40.757, 124.231)	<1	11	9	941
OR	Coos Bay Entrance	(43.353, 124.339)	1	13	8	2480
WA	Columbia River	(46.254, 124.026), (46.253, 123.563)	35, 2	14, 11	11, 10	1751, 689
WA	Grays Harbor	(46.917, 124.117)	11	9	8	576
WA	Haro Strait	(48.495, 123.154), (48.587, 123.218)	15, 15	276, 271	232, 199	625, 503
WA	Spieden Channel	(48.63, 123.126)	5	60	43	1893
WA	President Channel	(48.656, 123.139), (48.679, 122.999)	4, 4	54, 155	39, 129	1227, 528
WA	San Juan Channel	(48.547, 122.978)	7	93	62	1030
WA	Middle Channel	(48.459, 122.949)	8	93	60	2380
WA	Boundary Pass	(48.735, 123.061)	8	308	163	620
WA	Rosario Strait	(48.594, 122.755)	45	92	53	3349
WA	Bellingham Channel	(48.556, 122.658)	17	45	27	3077
WA	Guemes Channel	(48.523, 122.621)	2	8	7	1777
WA	Deception Pass	(48.407, 122.627)	2	6	6	1058
WA	Admiralty Inlet	(48.162, 122.737)	54	141	62	907
WA	Puget Sound	(47.591, 122.559)	2	22	11	2568
WA	Tacoma Narrows	(47.268, 122.544)	13	64	39	5602
WA	Dana Passage	(47.164, 122.862)	3	18	13	1851
AK	Bristol Bay	(58.604, 162.268), (58.532, 160.923) (58.442, 158.693)	160, 11, 304	48, 13, 19.9	28, 11, 12	5000, 654, 957
AK	Nushagak Bay	(58.975, 158.519)	122	14	8	2811
AK	Hague Channel	(55.908, 160.574)	1	24	17	564
AK	Herendeen Bay Entrance	(55.892, 160.793)	10	38	19	1564
AK	Moffet Lagoon Inlet	(55.446, 162.587)	1	7	7	845
AK	Izembek Lagoon	(55.328, 162.896), (55.248, 162.981)	<1, 1	8, 6	7, 6	539, 1606
AK	Bechevin Bay	(55.048, 163.45)	4	7	6	2252
AK	False Pass	(54.827, 163.384)	5	60	35	1619
AK	Unimak Pass	(54.333, 164.824)	132	82	57	830

Table 5 (*Continued*)

State	Hotspot	Location (°N, °W)	Surface area (km^2)	Maximum depth (m)	Mean depth (m)	Kinetic power density (W/m^2)
AK	Ugamak Strait	(54.168, 164.914)	63	88	48	1341
AK	Derbin Strait	(54.092, 165.235)	23	97	54	2348
AK	Avatanak Strait	(54.108, 165.478)	73	136	73	911
AK	Akutan Bay	(54.129, 165.649)	4	44	26	3365
AK	Akutan Pass	(54.025, 166.074)	50	83	49	2870
AK	Unalga Pass	(53.948, 166.21)	25	117	64	3751
AK	Umnk Pass	(53.322, 167.893)	97	138	56	2144
AK	Samalga Pass	(52.808, 169.122), (52.765, 169.346), (52.757, 169.686)	8, 138, 66	30, 277, 195	13, 103, 140	4102, 1718, 794
AK	Islands of Four Mountains	(52.862, 169.998)	7	147	53	2505
AK	Seguam Pass	(52.247, 172.673), (52.132, 172.826)	52, 128	190, 151	129, 85	800, 538
AK	Atka Island	(52.121, 174.065)	41	70	36	3444
AK	Fenimore Pass	(51.998, 175.388), (51.979, 175.477)	4, 28	95, 30	52, 16	2147, 1554
AK	Fenimore Pass	(51.974, 175.532), (51.961, 175.649)	3, 1	97, 25	50, 20	2410, 1304
AK	Chugul Island	(51.937, 175.755), (51.961, 175.866)	9, 9	100, 81	47, 48	1677, 1600
AK	Igitkin Island	(51.968, 175.974)	9	93	59	1110
AK	Unmak Island	(51.857, 176.066)	1	26	22	1155
AK	Little Tanaga Strait	(51.818, 176.254)	6	68	43	2276
AK	Kagalaska Strait	(51.79, 176.414)	1	20	18	758
AK	Adak Strait	(51.816, 176.982)	63	93	63	807
AK	Kanaga Pass	(51.723, 177.748)	36	55	29	889
AK	Delar of Islands	(51.677, 178.19), (51.55, 178.467), (51.564, 178.716), (51.586, 178.928)	83, 54, 8, 31	217, 102, 19, 126	78, 64, 11, 66	764, 649, 537, 1053
AK	Chirikof island	(55.964, 155.45)	198	44	31	597
AK	Tugidak Island	(56.294, 154.872)	284	51	26	681
AK	Sitkinak Island	(56.512, 154.383)	13	40	8	3104
AK	Aiaktalik Island	(56.639, 154.072), (56.738, 154.053)	79, 23	69, 33	28, 16	2497, 2038
AK	Moser Bay	(57.038, 154.115)	3	10	7	1874
AK	Kopreanof Strait	(57.934, 152.84), (57.987, 152.795)	17, 10	59, 21	29, 14	5454, 4636
AK	Shuyak Strait	(58.466, 152.496)	2	23	15	1007
AK	Stevenson Entrance	(58.647, 152.292), (58.663, 152.525)	33, 7	157, 75	102, 39	895, 779
AK	Barren Islands	(58.939, 152.127), (58.855, 152.345)	15, 9	115, 127	73, 78	686, 571
AK	Chugach Island	(59.091, 151.777), (59.12, 151.875), (59.148, 151.74), (59.163, 151.531), (59.082, 151.433)	34, 19, 15, 13, 20	116, 96, 90, 58, 64	54, 64, 26, 34, 47	587, 528, 1466, 916, 852
AK	Cook Inlet	(60.676, 151.58)	5285	140	34	5344
AK	Turnagain Arm	(60.978, 149.825), (60.982, 149.702), (60.998, 149.729)	8, 5, 2	13, 6, 5	9, 5, 5	3199, 657, 558
AK	Knik Arm	(61.385, 149.809), (61.396, 149.77), (61.41, 149.734), (61.428, 149.709), (61.371, 149.726)	4,2, 2, 3, 3	6, 5, 5, 7, 6	6, 5, 5, 6, 6	1993, 742, 749, 597, 1048
AK	Shelikof Strait	(58.239, 151.752)	15	31	24	524
AK	Montague Strait	(59.767, 147.966)	29	36	26	691
AK	Icy Strait	(58.353, 135.994)	274	287	94	8781
AK	Cross Sound	(58.223, 136.356), (58.225, 136.302), (58.256, 136.372), (58.288, 135.819)	3, 3, 1, 9	79, 139, 55, 124	72, 79, 46, 84	976, 503, 945, 513
AK	Adams Inlet	(58.863, 135.979)	4	16	9	1426
AK	Peril Strait	(57.455, 135.549), (57.371, 135.695)	1, 2	7, 43	7, 24	3285, 892
AK	Taku inlet	(58.384, 134.032)	4	14	10	864
AK	Seymour Canal	(57.922, 134.156), (57.93, 134.276)	<1, <1	14, 5	14, 5	770, 976
AK	Summer Strait	(56.369, 133.658), (56.437, 133.19), (56.441, 133.028)	11, 6, 4	185, 45, 184	67, 15, 101	1474, 801, 529
AK	Duncan Canal	(56.54, 133.088)	<1	37	37	604
AK	Kashevar of Passage	(56.233, 133.043), (56.269, 132.948)	6, 7	37, 109	27, 80	1039, 744
AK	Meares Passage	(55.259, 133.109)	1	17	14	1692



Fig. 4. Users can interact with tidal stream power map using the pull down menu or widgets on the right of the screen.

for a quick visual examination. On the other hand, the data points layer contains more detailed information that corresponds to actual model grid points and can be queried through the interactive tools, therefore, is more suited for in-depth analyses.

4.2. Identify tool

This tool is used to identify a single data point either by clicking on the map or by specifying a longitude and latitude. The identify tool returns the model water depth, mean/maximum tidal current magnitude, mean/maximum available kinetic power density and the exact longitude, latitude of the selected point. Detailed information about the related computational grid can also be accessed via the grid documentation link provided with this tool. The grid documentation includes a map showing the extent of the computational domain, and information on the model settings (boundary conditions, advection scheme, time step, bottom friction, etc.). The calibration statistics are also given in the grid documentation. Histograms for tidal current and tidal power density at a selected point can be plotted for any specific year using the identify tool. These histograms facilitate an overview of the nature of the tidal stream resource at a location as they display the total hours of availability for different ranges of specific current magnitude (or tidal power density) in a year. Similarly, time series for water surface elevation and tidal current speed plots and the associated data can be downloaded with the identify tool. An example for the year 2011 from a location at Cook Inlet, where model predicts strong currents is shown in Fig. 5. The identify tool suggests that the one-month mean tidal current magnitude is predicted to be 1.43 m/s, while the time series show the entire temporal variation in a year with a maximum that can be as high as 3.67 m/s. The histogram indicates that the current speed is larger than 0.5 m/s, 0.7 m/s and 1 m/s for more than 7442 h (310 days), 6885 h (286 days) and 5981 h (249 days) a year, respectively.

4.3. Select/export data tool

The select/export data tool is used to download data at selected grid points. A single point or multiple points can be selected using the select data tool via the selecting by dragging a window or selecting by polygon. The selected data can be filtered based on the water depth, mean current magnitude or mean power density or a combination of them prior to downloading. This provides the user with the option to only include the areas that meet certain criteria, such as a minimum depth or a minimum speed. The selected data is exported to a spreadsheet and for each point it includes all of the 67 columns that display geographical coordinates, the modeled depth, computed water level constituents and tidal current constituents, and one-month mean/maximum for tidal current speed and tidal stream power density.

Once the results are displayed in the identify or select/export widgets, the user can switch between the results and selection display using the top buttons on each widget. Instructions on how to use the web page, detailed project information, model documentation and contact information can be accessed through the help menu. The project information contains the background information, objectives and methodology. The computational model, generation of the grids and tidal forcing, calibration

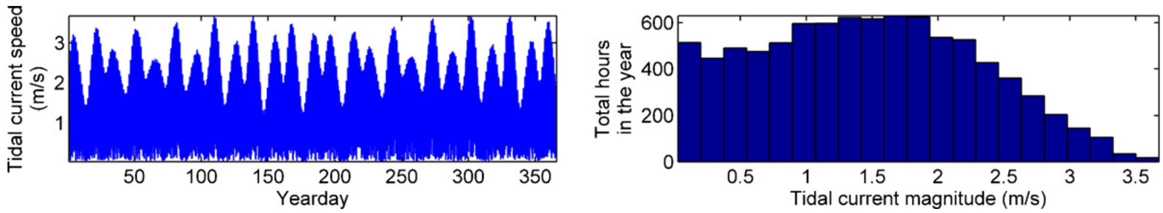


Fig. 5. An example of tidal current time series (left) and tidal current histogram (right) for a point selected with the identify tool.

and constituent extraction are explained under the model documentation.

5. Conclusion

A geodatabase of tidal constituents is developed to present the findings of a regional assessment of tidal stream power resources for the entire USA. The geodatabase is made accessible to the public through a spatial data server and interactive tools to select, query and download the data are provided. The results are based on numerical modeling of tidal currents with the purpose of regional assessment of the tidal steam power resource. The validation of the results with the measurements shows that the model predictions are good enough to meet the requirements for a regional assessment. However, a regional assessment needs to be followed by a pre-feasibility and a final feasibility study prior to a design development for the purpose of selecting a device and site development. These later stages focus on smaller regions than a nationwide scale of a regional study. It is possible to increase the accuracy of the in model predictions at these stages by grid refinement in areas along irregular coastlines and channel junctions where high spatial variability in flow features exist. In addition the spatial coverage of measurements can be increased by combining ship-mounted instrument data with the stationary point data.

A list of major hotspots for the largest kinetic power density in USA is given in this study. This list is obtained by filtering the regions with large tidal stream power density to satisfy the following criteria: (1) maximum of the average kinetic power density larger than 500 W/m^2 (corresponding to a current speed of ~1 m/s), (2) surface area larger than 0.5 km^2 and (3) depth larger than 5 m. The majority of the hotspots are found to be in Alaska. This is followed by Maine, Washington, Oregon, California, New Hampshire, Massachusetts, New York, New Jersey, North and South Carolina, Georgia, and Florida. The average tidal stream power density at some of these locations is larger than 8 kW/m^2 with surface areas on the order of few hundred kilometer squares, and depths larger than 100 m. Cook Inlet, Alaska is distinguished relative to the other hotspots with a large tidal stream power density sustained over an extraordinarily large area. The kinetic power density of tidal currents is a good indicator to locate tidal stream power resources, since tidal stream generators exploit the kinetic energy of moving water. However, the assessment of the upper bound for power conversion from tidal currents at these hotspots requires more detailed study as the overall power that can be converted from tidal streams is a function of both the kinetic and potential energy, and is also bound by environmental constraints and the effect of extraction on the flow itself. The environmental constraints include complex issues. For example, conflicts with existing uses, such as shipping and commercial fishing; performance of power converters in high suspended sediment and seasonal sea ice environments; changes to hydrodynamics and sediment transport and alterations to marine habitat and benthos, which are difficult to quantify due to knowledge gaps and a lack of clear monitoring protocols [36].

For further investigations of tidal stream power resources additional information can be integrated to the analysis. The choice of location for a tidal stream power converter farm depends on assessment of a number of criteria including the available power, site characteristics, and environmental, economic and social impacts of the planned project. These include available power and the site characteristics such as bathymetry, water depth and the geology of the seabed, changes in the flow patterns, water quality, sediment transport climates and related ecological impacts on the aquatic and terrestrial life, economic and social impacts based on the increased energy supply for the region and alterations to the marine and land use. Although it is not possible to quantify all of these criteria and there are no set rules on how to determine acceptable limits for many of them, certain GIS functionalities may be used to build a decision support system to select suitable locations for tidal stream power conversion [37]. A list of most suitable areas can be determined based on the level of power density, ease of accessibility and the number of environmental conflicts.

Acknowledgements

This study was supported by the Department of Energy, Wind and Hydropower Technologies Program award number DE-FG36-08GO18174. Any opinions, findings, and conclusions or recommendations expressed herein are those of the author(s) and do not necessarily reflect the views of the Department of Energy.

References

[1] Asif M, Muneer T. Energy supply, its demand and security issues for developed and emerging economies. Renewable and Sustainable Energy Reviews 2007;11:1388–413.
[2] Shafiee S, Topal E. When will fossil fuel reserves be diminished. Energy Policy 2009;37:181–9.
[3] USEPA. Inventory of U.S. greenhouse gas emissions and sinks: 1990–2009. EPA 430-R-11-005. U.S. Environmental Protection Agency; 2011.
[4] EMEC. Assessment of marine tidal energy resource. The European Marine Energy Centre Ltd.; 2009.
[5] Renewable resource maps. U.S. Department of Energy. http://www1.eere.energy.gov/maps_data/renewable_resources.html [accessed 2011].
[6] Bedard R, Previsic M, Polagye B, Hagerman G, Casavant A. North American tidal in stream energy conversion technology feasibility study. EPRI TP-008-NA. Electric Power Research Institute; 2006.
[7] Marine and hydrokinetic technology database. U.S. Department of Energy. http://www1.eere.energy.gov/windandhydro/hydrokinetic/default.aspx [accessed 2011].
[8] Haidvogel DB, Arango H, Budgell WP, Cornuelle BD, Curchitser E, Di Lorenzo E, et al. Ocean forecasting in terrain-following coordinates: formulation and skill assessment of the Regional Ocean Modeling System. Journal of Computational Physics 2008;227:3595–624.
[9] Defne Z, Haas KA, Fritz HM. Numerical modeling of tidal currents and the effects of power extraction on estuarine hydrodynamics along the Georgia Coast, USA. Renewable Energy 2011;36:3461–71.
[10] Sutherland DA, MacCready P, Banas NS, Smedstad LF. A model study of the Salish Sea estuarine circulation. Journal of Physical Oceanography 2011;41:1125–43.
[11] Coast Line Extractor. National Oceanic and Atmospheric Administration. http://rimmer.ngdc.noaa.gov/coast/ [accessed 2008].
[12] US Bathymetric & Fishing Maps. Office of Coast Survey, National Ocean Service, NOAA. http://map.ngdc.noaa.gov/website/mgg/fishmap/ [accessed 2008].
[13] Tides and currents. National Oceanic and Atmospheric Administration. http://tidesandcurrents.noaa.gov/index.shtml [accessed 2008].
[14] VDatum Vertical Datum Translator. NOAA's National Geodetic Survey (NGS), Office of Coast Survey (OCS), and Center for Operational Oceanographic Products and Services (CO-OPS). http://vdatum.noaa.gov/ [accessed 2008].
[15] Electronic Navigational Charts (ENC). Office of Coast Survey, National Oceanic and Atmospheric Administration. http://nauticalcharts.noaa.gov/mcd/enc/download.htm [accessed 2008].

[16] Geodas Grid Translator. National Geophysical Data Center. http://www.ngdc.noaa.gov/mgg/gdas/gd_designagrid.html [accessed 2008].
[17] National Wetlands Inventory. U.S. Fish & Wildlife Service. http://www.fws.gov/wetlands/ [accessed 2008].
[18] Seamless Server. U.S. Geological Survey. http://seamless.usgs.gov/ [accessed 2008].
[19] SeaGrid orthogonal grid maker for Matlab. U.S. Geological Survey. http://woodshole.er.usgs.gov/staffpages/cdenham/public_html/seagrid/seagrid.html [accessed 2008].
[20] Zevenbergen LW, Lagasse PF, Edge BL. Tidal hydrology, hydraulics, and scour at bridges. FHWA NHI-05-077. Ayres Associates; 2004.
[21] ADCIRC coastal circulation and storm surge model. http://www.unc.edu/ims/ccats/tides/tides.htm [accessed 2011].
[22] TPXO. Earth & Space Research. http://www.esr.org/polar_tide_models/Model_TPXO71.html [accessed 2011].
[23] Water data for the nation: National Water Information System. U.S. Geological Survey. http://waterdata.usgs.gov/usa/nwis/sw [accessed 2008].
[24] Chapman DC. Numerical treatment of cross-shelf open boundaries in a barotropic coastal ocean model. Journal of Physical Oceanography 1985;15:1060–75.
[25] Carter GS, Merrifield MA. Open boundary conditions for regional tidal simulations. Ocean Modelling 2007;18:194–209.
[26] Horizontal boundary conditions. WikiROMS. https://www.myroms.org/wiki/index.php/Boundary_Conditions#Horizontal_Boundary_Conditions [accessed 2011].
[27] Stewart K, Neary V. Validation of the Georgia Tech regional tidal current resource assessment model and GIS-web tool. Oak Ridge National Laboratory; 2011.
[28] Epler J. Tidal resource characterization from acoustic Doppler current profilers. Seattle: University of Washington; 2010.
[29] Myers L, Bahaj AS. Simulated electrical power potential harnessed by marine current turbine arrays in the Alderney Race. Renewable Energy 2005;30:1713–31.
[30] Lim YS, Koh SL. Analytical assessments on the potential of harnessing tidal currents for electricity generation in Malaysia. Renewable Energy 2010;35:1024–32.
[31] Fraenkel P. Marine current turbines: pioneering the development of marine kinetic energy converters. Proceedings of the Institution of Mechanical Engineers, Part A: Journal of Power and Energy 2007;221:159–69.
[32] Bedard R, Previsic M, Siddiqui O, Hagerman G, Robinson M. North American Tidal In Stream Energy Conversion Feasibility Demostration Project. EPRI TP-04-NA. Electric Power Research Institute; 2006.
[33] Lee MQ, Lu CN, Huang HS. Reliability and cost analyses of electricity collection systems of a marine current farm—a Taiwanese case study. Renewable and Sustainable Energy Reviews 2009;13:2012–21.
[34] Froberg E. Current Power Resource Assessment. Uppsala: Uppsala University; 2006.
[35] Assessment of energy production potential from tidal streams in the United States. Georgia Institute of Technology. http://www.tidalstreampower.gatech.edu/ [accessed 2011].
[36] Polagye B, Van Cleve B, Copping A, Kirkendall K. Environmental effects of tidal energy development. In: NOAA Technical Memorandum. NMFS F/SPO-116. U.S. Dept. Commerce; 2011.
[37] Defne Z, Haas KA, Fritz HM. GIS based multi-criteria assessment of tidal stream power potential: a case study for Georgia, USA. Renewable and Sustainable Energy Reviews 2011;15:2310–21.